Impact of Metallic Furniture on UWB Channel Statistical Characteristics

Chun-Liang Liu, Chien-Ching Chiu*, Shu-Han Liao and Yu-Shuai Chen

Department of Electrical Engineering, Tamkang University, Tamsui, Taiwan 251, R.O.C.

Abstract

The bit error rate (BER) performance for ultra-wide band (UWB) indoor communication with the impact of metallic furniture is investigated. The impulse responses of different indoor environments for any transmitter and receiver location are computed by shooting and bouncing ray/image and inverse fast Fourier transform (IFFT) techniques. By using the impulse responses of these multi-path channels, the BER performance for binary pulse amplitude modulation (BPAM) impulse radio UWB communication system are calculated. Numerical results have shown that the multi-path effect by the metallic cabinets is an important factor for BER performance. Also the outage probability for the UWB multi-path environment with metallic cabinets is larger than that with wooden cabinets. Finally, it is worth noting that in these cases the present work provides not only comparative information but also quantitative information on the performance reduction.

Key Words: UWB, BER, Outage Probability, RMS Delay Spread

1. Introduction

When the Federal Communications Commission (FCC) agreed in February 2002 to allocate 7.5 GHz spectrum for unlicensed use of ultra-wideband (UWB) devices for communications in the 3.1–10.6 GHz frequency band [1], the UWB technology has been the subject of extensive research in recent years due to its potential applications and unique capabilities. Low transmission power and short distance operation with UWB results in an extremely low transmitted power spectral density, which insures that impulse radio do not interfere with narrow-band radio systems operating in dedicated bands.

There are two basic methods to generate UWB signals. One way is to make use of orthogonal frequency division multiplexing (OFDM) in producing a GHz signal in frequency spectrum, the other way is impulse radio (IR) technology that directly produces a pulse, and this pulse's duration is only in the level of nanosecond [2,3]. Here, we motivate the suitability of IR UWB system that it offers many potential advantages, such as high resolution in multi-path reducing fading margins in link budget analysis, allowing for low transmit powers and low complexity.

All wireless systems must be able to deal with the challenges of operating over a multi-path propagation channel, where objects in the environment can cause multiple reflections to arrive at the receiver. BER degradation is caused by inter-symbol interference (ISI) due to a multi-path propagation made up of radio wave reflections by walls, floor, ceiling, laboratory fixtures. Generally, 100 Mbps transmission was actually confirmed to be available for an allowable BER of 10^{-5} [4–6].

Furthermore, while for continuous transmission multi-path causes rapid fluctuations in the received signal envelope and thus severe degradation in performance, in the IR UWB system, multiple paths reflect in a sequence of delayed and attenuated replicas of the transmitted pulse, which can eventually be successfully separated at the receiver. As a result, for IR UWB system, the effects

*Corresponding author. E-mail: chiu@ee.tku.edu.tw

of inter-symbol interference (ISI) can be degraded and improves BER performance further. Some literatures about BER performance for IR UWB system have been published [7–9], An analysis of ISI for an IR UWB symbol-differential autocorrelation receiver has been presented in [7]. In [8], a finite-resolution digital receiver design for impulse radio ultra-wideband communication has been investigated. A detection of impulse radio ultra-wideband signals using recursive transmitted reference receivers has been discussed in [9].

In this paper, we use ray tracing techniques and inverse fast Fourier transform (IFFT) to compute the impulse for UWB indoor communication, and the BER performance for binary pulse amplitude modulation (BPAM) impulse radio (IR) UWB system with the impact of metallic furniture is investigated. Channel modeling and system description is presented in section 2. Section 3 shows the numerical results. Finally, some conclusions are drawn in section 4.

2. Channel Modeling and System Description

The impulse response function for any transmitter-receiver location is computed as the following two steps: frequency responses for sinusoidal waves by SBR/Image techniques and inverse fast Fourier transform with Hermitian signal processing [10,11].

The shooting and bouncing ray (SBR)/Image method can deal with high frequency radio wave propagation in the complex indoor environments. It conceptually assumes that many triangular ray tubes are shot from the transmitting antenna (Tx) and each ray tube bouncing and penetrating in the environments is traced in indoor multi-path channel. The first order wedge diffraction is included, and the diffracted rays are attributed to corresponding image. Depolarization yielded by multiple reflections on walls and floors is also taken into account in our simulations.

The frequency responses are transformed to the time domain by using inverse fast Fourier transform with Hermitian signal processing. Using Hermitian signal processing, the pass-band signal is obtained with zero padding from the lowest frequency down to DC (direct current), taking the conjugate of the signal, and reflecting it to the negative frequencies. The result is then transformed to the time domain using IFFT. Since the signal spectrum is symmetric around DC. The resulting doubled-side spectrum corresponds to a real signal in time domain.

The equation used to model the multi-path radio channel is a linear filter with an impulse response given by

$$h_b(t) = \sum_{l=1}^{N} \alpha_l \delta(t - \tau_l) \tag{1}$$

where l is the path index, α_l is the path attenuation, τ_l is the time delay of the l th path and $\delta(\cdot)$ is the Dirac delta function. The goal of channel modeling is to determine the α_l and τ_l for each selected transmitter-receiver location.

The transmitted UWB pulse stream is [12]:

$$x(t) = \sqrt{E_{tx}} \sum_{i=0}^{\infty} p(t - iT_d)\ d \tag{2}$$

where T_p is the pulse duration and T_d is the duration of the transmitting signal ($T_d \gg T_p$). Binary PAM symbols $d \in \{\pm 1\}$ are assumed to be independent identically distributed (i.i.d.). The diagram of transmitted waveform is shown in Figure 1; the second derivative Gaussian waveform *p(t)* has ultra-short duration T_p at the nanosecond scale. The second derivative Gaussian waveform *p(t)* can be described by the following expression:

$$p(t) = \frac{d^2}{dt^2}\left(\frac{1}{\sqrt{2\pi}\sigma} e^{\frac{-t^2}{2\sigma^2}}\right) \tag{3}$$

where t and σ are time and standard deviation, respectively. The average transmit energy symbol E_{tx} can be expressed as

$$E_{tx} = \int_0^{T_d} p^2(t)dt \tag{4}$$

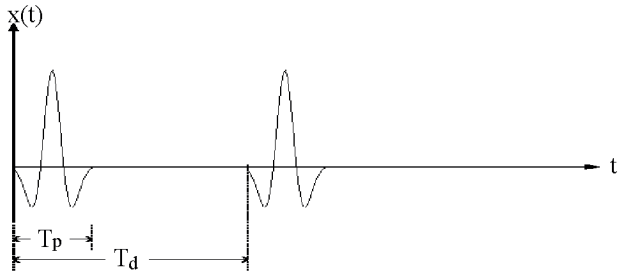

Figure 1. The diagram of transmitted waveform.

Block diagram of the simulated communication system is shown in Figure 2. The transmitted signal after propagating through channel, the received signal takes on the general form as

$$r(t) = [x(t) \otimes h_b(t)] + N(t) \tag{5}$$

where $\otimes$ is defined as convolution.

The correlation receiver samples the received signal at the symbol rate and correlates them with suitably delayed references given by

$$q(t) = \sum_{n=0}^{\infty} p(t - \tau_1 - (n-1)T_d) \tag{6}$$

where τ_1 is the delay time ofthe first wave, received by the receiver.

The output of the correlator is [13,14]

$$\begin{aligned} Z(n) = & \int_{(n-1)T_d}^{nT_d} \left\{ [\sqrt{E_{tx}} \sum_{i=0}^{\infty} p(t - iT_d)d] \otimes h_b(t) \right\} \\ & \cdot q(t)dt + \int_{(n-1)T_d}^{nT_d} N(t)q(t)dt = V(n) + \eta(n) \end{aligned} \tag{7}$$

Z(n) is then compared with a threshold set at zero, a decision being made in favor of a "1" or a "-1", depending on whether Z(n) is positive or negative, respectively. It can be shown that the noise components η(t) of Eq. (7) are uncorrelated Gaussian variables with zero mean. The variance of the output noise η is

$$\sigma^2 = \frac{N_0}{2} E_{tx} \tag{8}$$

The average probability of error on the bit is thus expressed by:

$$P[Z(n) \mid \vec{d}] = \frac{1}{2} erfc\left[\frac{V(n)}{\sqrt{2}\sigma} \cdot (d_N) \right] \tag{9}$$

where $erfc(x) = \frac{2}{\sqrt{\pi}} \int_x^{\infty} e^{-y^2} dy$ is complementary error function and $\vec{d} = d_1, d_2, \ldots, d_N$ is the binary sequence.

Finally, the BER for IR-UWB system can be expressed as

$$BER = \sum_{n=1}^{N} P(\vec{d}) \cdot \frac{1}{2} erfc\left[\frac{V(n)}{\sqrt{2}\sigma} \cdot (d_N) \right] \tag{10}$$

where $P(\vec{d})$ is the occurring probability of the binary sequence $\vec{d}$.

3. Numerical Results

Since the dielectric permittivity and the loss tangent of the materials changes with frequency, the different values of dielectric constant and loss tangent of materials for different frequency are carefully considered in channel calculation [15]. For example, the dielectric constant and loss tangent of wood are shown in Table 1.

Figure 3(a) and Figure 3(b) the 3D perspective and

Table 1. The dielectric constant and loss tangent of wood

Frequency (GHz)	Dielectric Constant	Loss Tangent
3.0	2.17	4.61E-01
3.5	2.15	4.41E-01
4.0	2.14	4.25E-01
4.5	2.13	4.13E-01
5.0	2.12	4.03E-01
5.5	2.10	3.94E-01
6.0	2.10	3.87E-01
6.5	2.09	3.81E-01
7.0	2.09	3.75E-01
7.5	2.08	3.70E-01
8.0	2.08	3.66E-01
8.5	2.08	3.62E-01
9.0	2.07	3.56E-01
9.5	2.07	3.53E-01
10.0	2.07	3.49-01

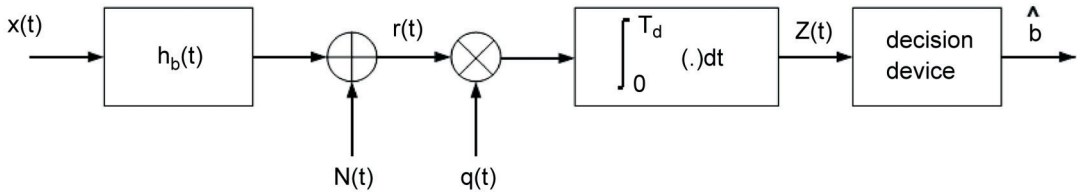

Figure 2. Block diagram of the simulated communication system.

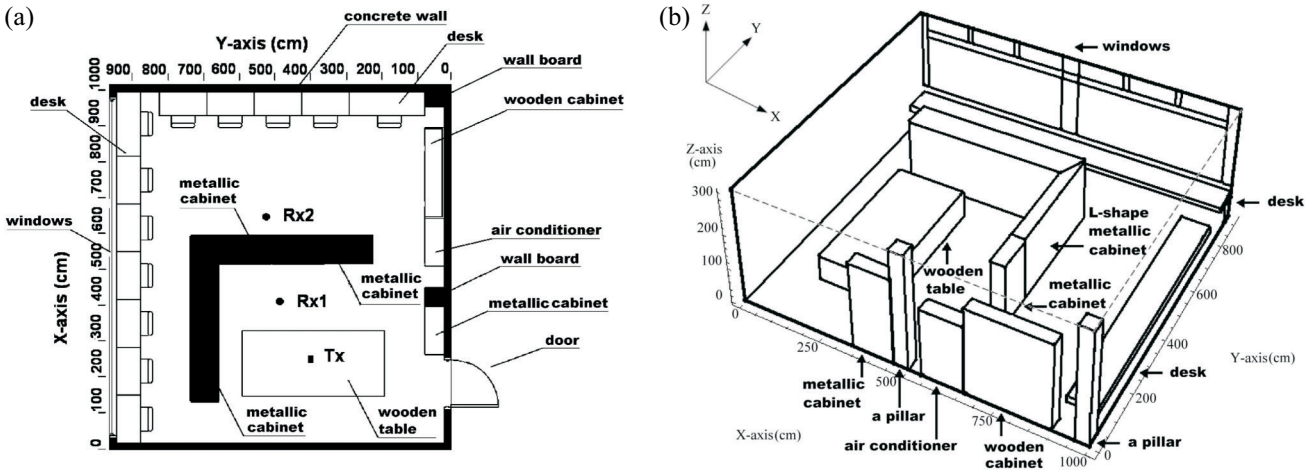

Figure 3. (a) 3D perspective of the Microwave laboratory in Tamkang University. (b) Top view of the Microwave laboratory in Tamkang University and this laboratory has dimensions of 9.2 m (Length) × 10 m (Width) × 3 m (Height). The transmitter is located at Tx (250, 400, 120) cm, the receiver are located at R × 1 (400, 500, 75) cm and R × 2 (650, 525, 75) cm.

top view of Microwave Laboratory in Tamkang University respectively. The laboratory has dimensions of 9.2 m (length) × 10 m (width) × 3 m (height). The laboratory with L-shape metallic cabinet or L-shape wooden cabinet is considered in the simulation. The transmitting and receiving antennas are both short dipoles and vertically polarized. The transmitting antenna Tx (250, 400, 120) cm is located on the center of the wooden table in the Microwave laboratory. 1250 different locations of receiver antenna with uniformly distributed in the laboratory are chosen for simulations. There are 574 and 676 receiving points for line-of-sight (LOS) and non-line-of-sight (NLOS) cases respectively .Meanwhile the receiver antenna at R × 1 (400, 500, 75) cm and R × 2 (650, 525, 75) cm are also plotted in Figure 3(b) for the further discuss. The maximum number of bounces setting beforehand is four, and the convergence is confirmed.

Figure 4(a) and Figure 4(b) compare the impulse responses at R × 1 located in front of the L-shape metallic and wooden cabinet respectively. Simulation results show that the impulse response in Figure 4(a) quite matches to that in Figure 4(b) in the early time response, due to the fact that both Figure 4(a) and Figure 4(b) have LOS waves. However, for the late time response, the multipath effect for the metallic cabinet is more severe than that for the wooden cabinet.

Figure 5(a) and Figure 5(b) compare the impulse response at R × 2 located in the back of the L-shape metallic cabinet and wooden cabinet. Simulation results show that the impulse response in Figure 4(a) is almost zero in the early time. Compared to that in Figure 4(b), the impulse response exists in the early time because the signal can transmit through the wooden cabinet. In addition, the impulse response in Figure 4(a) is similar to that in Figure 4(b) in the late time response, due to the transmission environment except L-shape cabinet is the same for Figure 5(a) and Figure 5(b). It is also seen that the multi-path with metallic cabinets is more serious than that with wooden cabinet, due to the fact that radio wave can penetrate through the wooden cabinet and is blocked by the metallic cabinet.

Figure 6 shows the cumulative distribution function of RMS delay spreads for LOS and NLOS waves with L-shape wooden and metallic cabinets respectively. The root mean square (RMS) delay spread τ_{rms} is defined as follows:

$$\tau_{rms} = \sqrt{\frac{\sum_{l=1}^{N} \tau_l^2 |\alpha_l|^2}{\sum_{l=1}^{N} |\alpha_l|^2} - \left(\frac{\sum_{l=1}^{N} \tau_l |\alpha_l|^2}{\sum_{l=1}^{N} |\alpha_l|^2} \right)^2} \tag{11}$$

Equation (11) measures the effective duration of the channel impulse response. It is a fundamental parameter for evaluating the presence of ISI at the receiver. If the time interval separating two pulses is smaller than τ_{rms}, ISI is present. The mean value and standard deviation of RMS delay spreads is shown in Table 2. The mean RMS

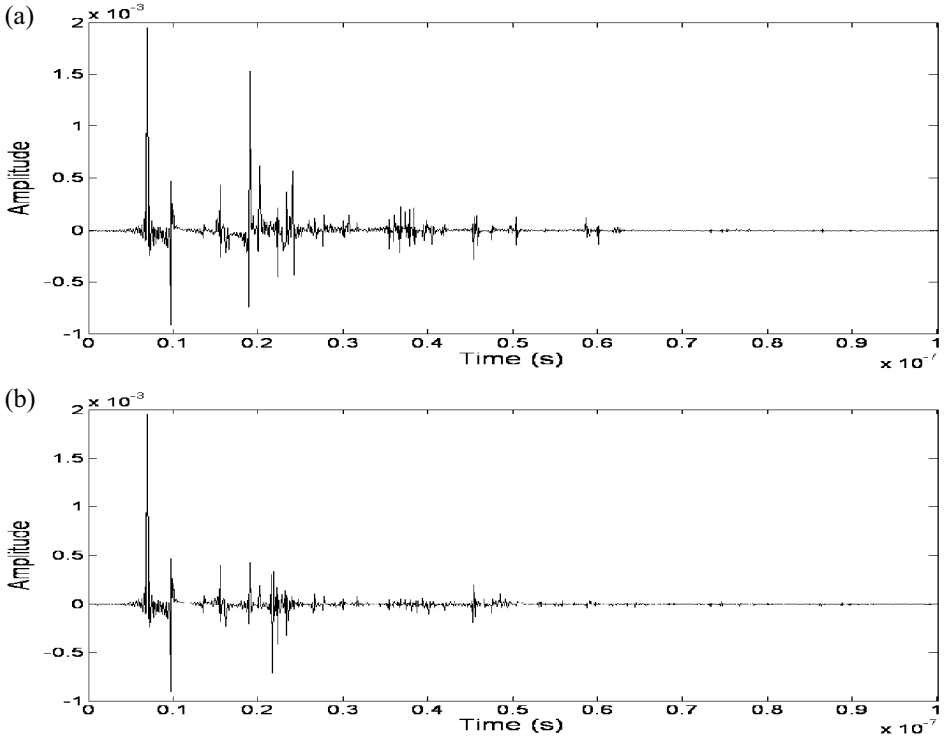

Figure 4. (a) The impulse response at R × 1 located in front of the L-shape metallic cabinet. (b) The impulse response at R × 1 located in front of the L-shape wooden cabinet.

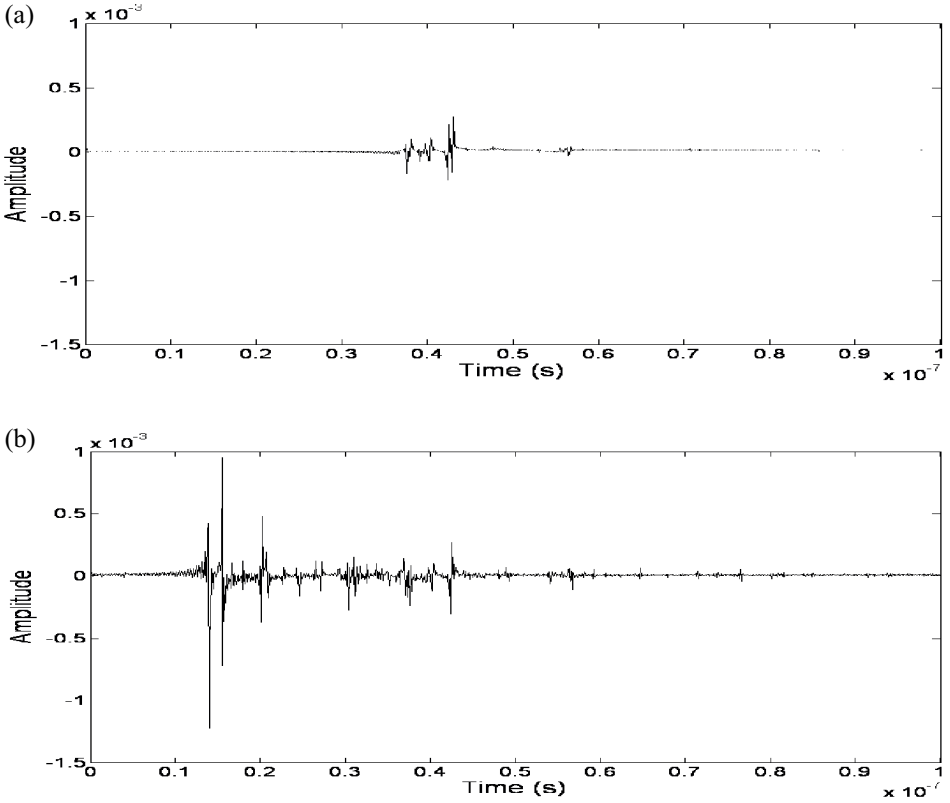

Figure 5. (a) The impulse response at R × 2 located behind the L-shape metallic cabinet. (b) The impulse response at R × 2 located behind the L-shape wooden cabinet.

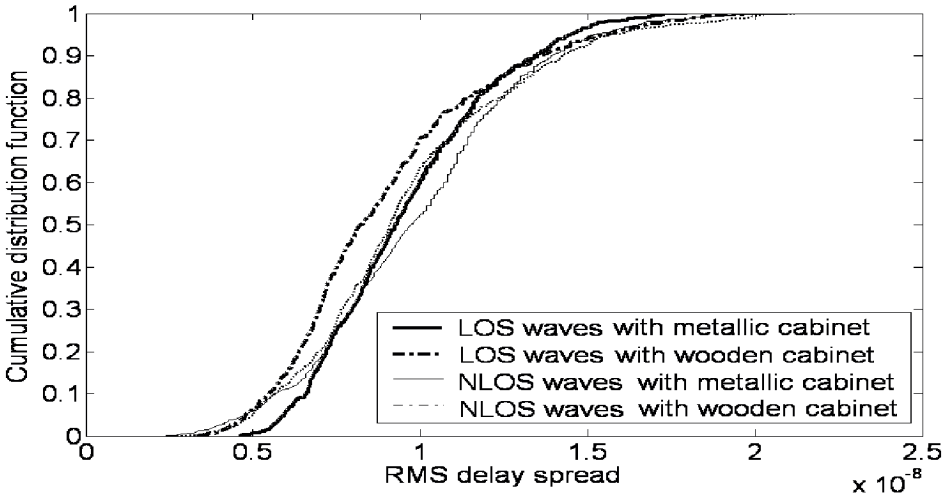

Figure 6. Cumulative distribution function versus RMS delay spread with LOS and NLOS waves.

Table 2. RMS delay spread with LOS and NLOS waves

RMS delay spread	LOS waves (metallic cabinet)	LOS waves (wooden cabinet)	NLOS waves (metallic cabinet)	NLOS waves (wooden cabinet)
Mean (sec)	9.61E-09	8.98E-09	9.84E-09	9.63E-09
Standard Deviation	2.63E-09	3.21E-09	3.23E-09	3.35E-09

delay spread is 9.61 ns and 8.98 ns for the L-shape metallic cabinet and wooden cabinet respectively for LOS cases. It is also seen the mean RMS delay spread is 9.84 ns and 9.63 ns for the L-shape metallic cabinet and wooden cabinet respectively in NLOS case. It is clear that the multi-path effect for the metallic cabinet is severe than that for the wooden cabinet.

Figure 7 shows the bit error rate (BER) versus signal-to-noise rate (SNR) for receivers at Rx1 and R × 2. Here SNR is defined as the ratio of the average power to the noise power at the front end of the receiver. For a BER = 10^{-5} and the receiver antenna at R × 2 located behind of the cabinet, the SNR value for metallic cabinet is larger than that for the wooden cabinet about 6 dB. This is due to the fact that radio wave can pass through the wooden cabinet and is blocked by the metallic cabinet.

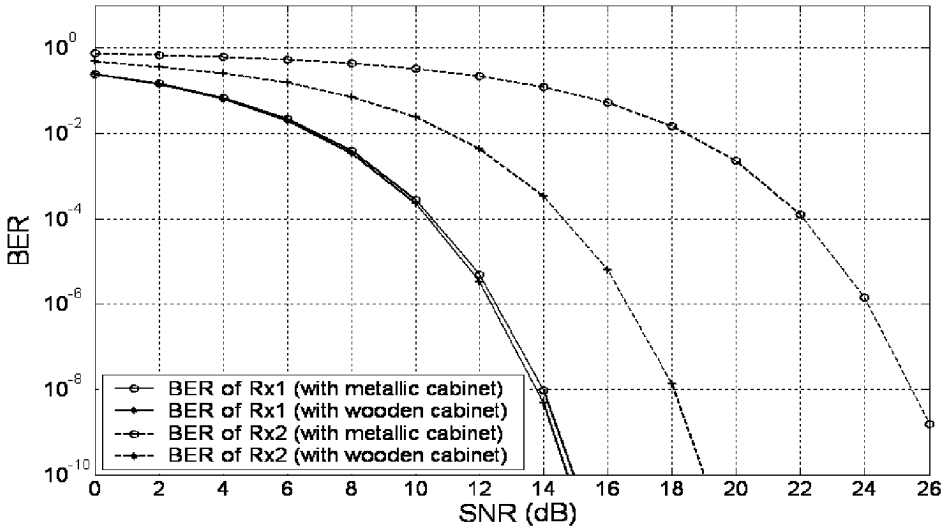

Figure 7. BER performance for the metallic and wooden cabinets.

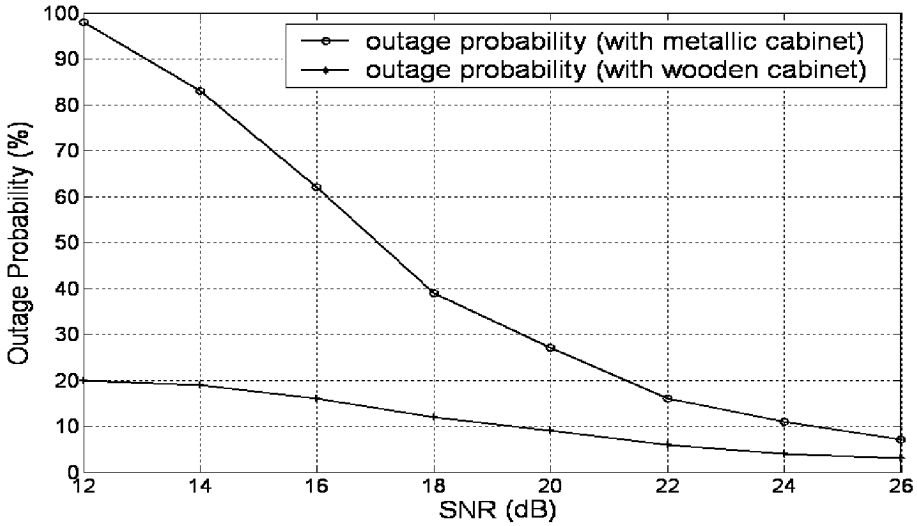

Figure 8. Outage probability versus SNR for a system with 1250 receivers.

Furthermore, for the wooden cabinet, the SNR value at R × 2 is larger than that at R × 1 about 4 dB, due to R × 1 has a LOS wave and R × 2 has only NLOS waves. Finally, the performance at R × 2 located in back of the metallic cabinet become worse while comparing with the R × 1.

Figure 8 shows the outage probability versus SNR. At 100 M bps transmission rate, the outage probabilities depicted in Figure 8 for a BER < 10^{-5} and SNR = 20 dB are about 27.4% and 9.3% for the metallic and wooden cabinets respectively. It is clear that the BER performance for the wooden cabinet is better due to the less severe multi-path effect.

4. Conclusion

The BER performance for IR-UWB indoor communication with metallic and wooden cabinet has been investigated. By using the impulse response of the multi-path channel, the BER for high-speed UWB indoor communication has been calculated. The impact of metallic cabinet to indoor multi-path is presented and the channel statistical characteristics are analyzed. Moreover, the frequency dependence of materials utilized in the structure on the indoor channel is accounted for in the channel simulations.

Numerical results show that the outage probability for the UWB multi-path environment with metallic cabinets is larger than that with wooden cabinet. This is due to the fact that the multi-path effect is severe when metallic cabinets exist in the room. Finally, it is worth noting that in these cases the present work provides not only comparative information but also quantitative information on the performance reduction.

References

[1] First report and order, revision of part 15 of the communication's rules regarding ultra-wideband transmission systems, FCC, ET Docket, pp. 98–153 (2002).

[2] Siwiak, K., Withington, P. and Phelan, S., "Ultra-Wide Band Radio: The Emergence of an Important New Technology," *IEEE VTS 53rd Vehicular Technology Conference,* Vol. 2, pp. 1169–1172 (2001).

[3] Siwiak, K., "Ultra-Wide Band Radio: Introducing a New Technology," *IEEE VTS 53rd Vehicular Technology Conference,* Vol. 2, pp. 1088–1093 (2001).

[4] Mielczarek, B., Wessman, M. O. and Svensson, A., "Performance of Coherent UWB Rake Receivers with Channel Estimators," *IEEE 58th Vehicular Technology Conference,* pp. 1880–1884 (2003).

[5] Hamalainen, M. and Iinatti, J., "Analysis of Interference on DS-UWB System in AWGN Channel," *2005 IEEE International Conference on Ultra-Wideband,* pp. 719–723 (2005).

[6] Kandukuri, S. and Boyd, S., "Optimal Power Control in Interference-Limited Fading Wireless Channels with Outage-Probability Specifications," *IEEE Transactions on Wireless Communications,* pp. 46–55 (2002).

[7] Pausini, M., Janssen, G. and Witrisal, K., "Analysis of ISI for an IR UWB Symbol-Differential Autocorre-

lation Receiver," Vehicular Technology Conference, 2004. *VTC2004-Fall. 2004 IEEE 60th,* Vol. 2, pp. 1213–1217V (2004).

[8] Ke, L., Wang, Z., Yin, H. and Gong, W., "Finite-Resolution Digital Receiver Design for Impulse Radio Ultra-Wideband Communication," *IEEE International Conference on communications,* pp. 845–849 (2008).

[9] Khan, M. G., Nordberg, J. and Claesson, I., "Detection of Impulse Radio Ultra-Wideband Signals Using Recursive Transmitted Reference Receivers," *IEEE International Conference on Ultra-Wideband,* pp. 376–380 (2007).

[10] Chen, S. H. and Jeng, S. K., "An SBR/Image Approach for Indoor Radio Propagation in a Corridor," *IEICE Trans. Electron,* E78-C, pp. 1058–1062 (1995).

[11] Chen, S. H. and Jeng, S. K., "SBR/Image Approach for Indoor Radio Propagation in Tunnels with and without Traffic," *IEEE Trans. Veh. Technol,* Vol. 45, pp. 570–578 (1996).

[12] Tian, Z. and Giannakis, G. B., "BER Sensitivity to Mistiming in Ultra-Wideband Impulse Radios-Part I: Nonrandom Channels," *IEEE Transactions on Signal Processing,* pp. 1550–1560 (2005).

[13] Homier, E. A. and Scholtz, R. A., "Rapid Acquisition of Ultra-Wideband Signals in the Dense Multipath Channel," *IEEE Conference on Ultra Wideband Systems and Technologies,* pp. 105–109 (2002).

[14] Gargin, D. J., "A Fast and Reliable Acquisition Scheme for Detecting Ultra Wide-Band Impulse Radio Signals in the Presence of Multi-Path and Multiple Access Interference," *2004 International Workshop on Ultra Wideband Systems,* pp. 106–110 (2004).

[15] Imada, S. and Ohtsuki, T., "Pre-RAKE Diversity Combining for UWB Systems in IEEE 802.15 UWB Multipath Channel," IEEE Joint with Conference on Ultrawideband Systems and Technologies. Joint UWBST & IWUWBS. *2004 International Workshop on Ultra Wideband Systems,* pp. 236–240 (2004).

Manuscript Received: Nov. 6, 2007
Accepted: Oct. 9, 2008